Comparing upper tropospheric humidity data from microwave satellite instruments and tropical radiosondes

Isaac Moradi[1], Stefan A. Buehler[1], Viju O. John[2], and Salomon Eliasson[1]

I. Moradi, Satellite Atmospheric Science Group, Department of Space Science, Luleå University of Technology, Box 812, Kiruna 98128, Sweden. Email: isaac.moradi@ltu.se

S. A. Buehler, Satellite Atmospheric Science Group, Department of Space Science, Luleå University of Technology, Box 812, Kiruna 98128, Sweden. E-mail: sbuehler@ltu.se

V. O. John, Met Office Hadley Centre, FitzRoy Road Exeter EX1 3PB UK. E-mail: viju.john@metoffice.gov.uk

S. Eliasson, Satellite Atmospheric Science Group, Department of Space Science, Luleå University of Technology, Box 812, Kiruna 98128, Sweden. E-mail: s.eliasson@ltu.se

[1]IRV, Luleå University of Technology,

Kiruna, Sweden

[2]Met Office Hadley Centre, Exeter, UK

Abstract. Atmospheric humidity plays an important role in the Earth's climate. Microwave satellite data provide valuable humidity observations in the upper troposphere with global coverage. In this study, we compare upper tropospheric humidity (UTH) retrieved from the Advanced Microwave Sounding Unit (AMSU-B) and the Microwave Humidity Sounder (MHS) against radiosonde data measured at four of the central facilities of the Atmospheric Radiation Measurement (ARM) program. The Atmospheric Radiative Transfer Simulator (ARTS) was used to simulate satellite brightness temperatures from the radiosonde profiles. Strong ice clouds were filtered out, as their influence on microwave measurements leads to incorrect UTH values. Day and night radiosonde profiles were analyzed separately, to take into account the radiosonde radiation bias. The comparison between radiosonde and satellite is most meaningful for data in cloud free, night time conditions, and with a time difference of less than 2 hours. We found good agreement between the two data sets. The satellite data are slightly moister than the radiosonde data, with a mean difference of $1 - 2.3\,\%$RH, depending on the radiosonde site. Monthly gridded data were also compared, and showed slightly larger mean difference of up to $3.3\,\%$RH, which can be explained by sampling issues.

1. Introduction

Atmospheric water vapor is the main natural greenhouse gas and enhances the sensitivity of the climate to global warming by about 70%, hence playing an important role in climate change prediction [*Cess et al.*, 1990]. Global climate models that contain water vapor feedback with an approximately constant relative humidity in a warming climate, predict that over the next century the Earth's surface will warm nearly twice as much as models that do not contain water vapor feedback [*Minschwaner and Dessler*, 2004]. The middle and upper troposphere contribute strongly to the water vapor feedback, especially in the tropics, owing to the low temperatures at these altitudes.

The water vapor feedback mechanism in the upper troposphere appears to be in reasonable agreement both between different climate models [e.g., *John and Soden*, 2007] and between models and observations [e.g., *Gettelman and Fu*, 2008]. However, as shown for example by *John and Soden* [2007], the absolute values of upper tropospheric humidity (UTH) disagree significantly between different models.

Although a number of studies have analyzed the distribution of water vapor in the upper troposphere [e.g., *Gettelman et al.*, 2006; *Gettelman and Fu*, 2008; *Soden et al.*, 2005; *Buehler et al.*, 2008], large uncertainties remain in the available upper tropospheric humidity (UTH) data sets [*de F. Forster and Collins*, 2004].

Two main sources of UTH information are radiosondes and satellite observations. The radiosonde data have been available since the 1940s from synoptic stations, but the data quality in the upper troposphere is questionable [*Elliott and Gaffen*, 1991]. In contrast to radiosonde measurements, satellite data have global coverage but these observations

are available only since 1979 from infrared (IR) sounders (6.7 μm band) and since 1994 from microwave sounders (183.31 GHz). The IR channels are heavily influenced by clouds, whilst microwave measurements are less sensitive to clouds [*Buehler et al.*, 2007].

The first attempt to relate infrared radiances (T_b) to UTH was made by *Soden and Bretherton* [1993]. They presented a linear relation (see Equation 1) between the brightness temperature of the 6.7 μm band from GOES–7 and Jacobian weighted relative humidity in the upper troposphere (approximately $500 - 200$ hPa). They stated that the accuracy is within ± 1 K or ± 10 %RH. *Buehler and John* [2005] adapted this brightness temperature transformation method to AMSU-B data, hereafter referred to as AMSU, to retrieve Jacobian weighted UTH. A global UTH dataset, derived from radiances of the AMSU instruments on-board the satellites NOAA-15, -16 and -17, hereafter referred to as N15, N16, and N17, respectively, is described in *Buehler et al.* [2008] (An updated version of the data set is available at `http://www.sat.ltu.se/projects/uth-clim/`).

AMSU data have previously been compared to European radiosonde data [e.g., *Buehler and John*, 2005; *John and Buehler*, 2005; *Buehler et al.*, 2008], but the focus has never been in the tropics. UTH in the tropics is of large importance to the Earth's climate system. In light of this, we use data from the atmospheric radiation measurement (ARM) program [*Stokes and Schwarts*, 1994] measured at the Tropical Western Pacific (TWP) stations, located near the equator, and the sub-tropical Southern Great Plains (SGP) station in this study. The measurements are made using high quality modern sensors with good calibration and good vertical resolutions. The aim of this study is to evaluate the capability of microwave satellite data to retrieve upper tropospheric humidity in the

tropics. A secondary aim is to evaluate the homogeneity and data quality of the ARM radiosonde data set.

The structure of the article is as follows: Section 2 provides information about the satellite and radiosonde data, focusing on the data properties relevant for the comparison. Section 3 presents the RT model, the UTH retrieval from satellite data, the cloud filter used, and the method used to collocate satellite and radiosonde data. Section 4 investigates and explains the results of the comparisons of the individual data and monthly mean data respectively, and Section 5 presents the conclusions.

2. Measurements

2.1. Satellite Data

The Advanced Microwave Sounding Unit-B (AMSU-B) is a cross-track scanning 5 channel (16–20, channels 1–15 are of AMSU-A) microwave radiometer. The AMSU-B channels operate at 89.0, 150.0, 183.31 ± 1.00, 183.31 ± 3.00, and 183.31 ± 7.00 GHz. The instrument has a swath width of approximately 2300 km, with 90 scan positions. The satellite viewing angle is 0.55° from nadir for the innermost scan positions, and 48.95° from nadir for the outermost scan positions. This corresponds to incidence angles of 0.62° and 58.5° from nadir, respectively. The AMSU-B footprint size, defined with respect to the half power beam width, is approximately 15 km at nadir but increases towards the edge of the scan [*Saunders et al.*, 1995; *Goodrum et al.*, 2007].

The AMSU-B instruments are onboard the NOAA-15, -16, and -17 satellites. The NOAA-18, -19 and Metop-A satellites, hereafter referred to as N18, N19 and MA, respectively, have the Microwave Humidity Sounder (MHS) on-board, instead of AMSU-B. MHS is very similar to the AMSU-B, but the second channel has moved to 157.0 GHz and the

fifth channel has only one passband at 190.311 GHz [*Bonsignori*, 2007; *Goodrum et al.*, 2007]. In this study AMSU-B data from all available satellites and MHS data from N18 and MA are used.

2.2. ARM Dataset

The Atmospheric Radiation Measurement (ARM) Program is a global change research program supported by the U.S. Department of Energy (DOE) since 1989. The primary goal of the ARM Program is to improve the understanding of the fundamental physics of the interaction between clouds and radiative feedback processes in the atmosphere. A typical radiosonde provides vertical profiles of both the thermodynamic state of the atmosphere, and the wind speed and direction. Radiosonde data of ARM include moisture, pressure, temperature and horizontal wind.

Radiosonde data from the Tropical Western Pacific (TWP-C1, -C2, and -C3) and Southern Great Plains (SGP-C1) stations are used in this study. These are located at Lamont, Manus, Naura Island and Darwin, respectively. The station details are shown in Table 1 and Figure 1. The TWP stations, especially TWP-C1 and TWP-C2, are particularly close to the equator and are located in a tropical convective zone. Table 2 shows details of the radiosonde sensors, including the time period used in this study. Radiosonde data used in this study are mostly from Vaisala RS92 sensors. RS92 has two humidity sensors, where one is heated while the other measures. This eliminates condensation on the sensors when inside clouds or due to prolonged exposure to super-saturation. However, RS92 radiosondes suffer from a radiation dry bias when exposed to sunlight [*Vömel et al.*, 2007]. This is believed to be caused by their lack of a radiation shield and by their large surface area due to the dual sensors.

In the lower troposphere the daytime dry bias was estimated to be $3-4\%$ for RS80 [*Turner et al.*, 2003], and $6-8\%$ for RS90/92 [*Miloshevich et al.*, 2006b] based on comparisons to ground based microwave radiometer precipitable water measurements. *Vömel et al.* [2007] found the RS92 day-time bias to increase with altitude to up to 50% near 16 km. For the altitude region that Channel 18 of AMSU-B is sensitive to ($5-10$ km), the dry bias ranges from $10-30\,\%$.

3. Methodology

We use the profile-to-satellite approach, described for example in *Soden and Lanzante* [1996] and in *Buehler et al.* [2004], where satellite radiances are simulated from radiosonde profiles. The same transformation is then applied to both measured and simulated radiances to convert the data to UTH. This approach avoids inconsistencies due to the varying vertical sampling of the satellite.

3.1. ARTS Model

The Atmospheric Radiative Transfer Simulator (ARTS) [*Buehler et al.*, 2005] was used to simulate AMSU/MHS radiances from radiosonde profiles. The ARTS setup for AMSU/MHS simulation has been discussed by *Buehler et al.* [2004].

Radiosonde data above 100 hPa are discarded, to maintain a homogeneous vertical extent. This introduces a bias of approximately $0.033-0.090$ K, depending on the channel, with a small random error of $0.006-0.057$ K [*Buehler et al.*, 2004]. Radiosonde profiles that do not contain data up to 100 hPa are not used in the study. This filters out about 5% of the SGP-C1 profiles, 8% of the TWP-C1 and -C2 profiles and 4% of the TWP-C3 profiles.

The vertical profiles of air pressure, temperature and water vapor volume mixing ratio are used as input to ARTS. The ARM radiosonde data do not include ozone concentrations therefore, radiances are calculated without the impact of ozone. The impact of this omission on AMSU radiances is estimated to be largest for Channel 18, with a maximum impact of 0.5 K [*John and Buehler*, 2004].

3.2. Retrieving UTH from AMSU/MHS Data

Following *Buehler and John* [2005], the linear relationship shown below is used to estimate UTH from the 183.31 ± 1.00 GHz radiances:

$$\ln(\mathrm{UTH}) = a + b \cdot T_b \tag{1}$$

where, T_b is the radiance expressed in brightness temperature and a and b are linear fit coefficients which are available separately for all viewing angles [see *Buehler and John*, 2005] so that radiances do not need to be limb corrected [*John et al.*, 2006].

3.3. Co-locating Satellite and Radiosonde Data

A radiosonde balloon typically drifts about 50 km horizontally while ascending from the ground to 100 hPa. Hence the average T_b of a target area, rather than that of an individual pixel, is compared to the radiosonde simulated radiance [*Buehler et al.*, 2004]. The target area is defined by a circle of radius 50 km from the launch site, which normally encompasses around 10–30 pixels. The pixels inside the target area have different viewing angles, and therefore the radiosonde brightness temperature is also simulated for the corresponding viewing angles. On average, a radiosonde takes about 20 minutes to reach 500 hPa and about $45 - 60$ minutes to reach 200 hPa. Therefore the radiosonde-time used to collocate with satellite data is defined as its launch time plus 45 minutes. The displacement of the

air mass at this time is also considered. Radiosonde wind data between 700 and 300 hPa, the altitude range most important for the humidity channels, are used to calculate the average wind vector. The average wind vector is multiplied by the time difference between the satellite overpass and radiosonde-time. If the calculated displacement is larger than 50 km, the data are excluded [*Buehler et al.*, 2004]. In addition, the acceptable time difference between satellite overpasses and radiosonde-times is limited to two hours. The numbers of clear-sky, night-time collocations are given in Table 3

3.4. Cloud Filtering Method

Microwave radiances are less sensitive to clouds than infrared radiances, but sufficiently optically thick ice clouds can affect microwave data. A cloud filter introduced by *Buehler et al.* [2007] was used to exclude cloud affected pixels from AMSU/MHS data. The cloud filter as follows. Firstly, Channel 18 of AMSU/MHS is sensitive to higher altitudes of the troposphere than Channel 20. In clear-sky conditions, because of the natural lapse rate of air temperature, brightness temperature of Channel 18 (T_B^{18}) is colder than brightness temperature of Channel 20 (T_B^{20}). Ice clouds scatter outgoing radiation and reduce T_B^{20} more strongly than T_B^{18}. Therefore, in the presence of an ice cloud $\Delta T_B = T_B^{20} - T_B^{18}$, which is positive in clear-sky conditions, becomes negative. Secondly, the cloud also reduces the value of T_B^{18} directly, so that a viewing angle dependent threshold $T_{thr}(\theta)$ was utilized. In summary, the conditions for clear-sky data are $\Delta T_B > 0$ and $T_B^{18} > T_{thr}(\theta)$. Data not fulfilling both conditions are considered cloudy. Values of T_{thr} for different viewing angle are given in *Buehler et al.* [2007]. The performance of this method for tropical regions will be discussed in Section 4.1.

4. Results and Discussion

Figure 2 shows scatter plots of collocated N17, AMSU-B Channel 18 T_b data versus TWP-C1 simulated brightness temperatures for this channel. This figure includes separate plots for night-time all skies (subplot (a)), night-time cloud-free (subplot (b)) and day-time cloud free (subplot (c)) data. Each data point corresponds to the average value in the target area as discussed in Section 3.3. Vertical lines represent the standard deviations of AMSU-B pixels inside the target area. These represent the inhomogeneity of the atmosphere observed by the satellite. This quantity is used to weight data for calculating statistics, such as bias and linear fit parameters, where a high standard deviation corresponds to a small weight. (See Appendix A for details.)

4.1. Cloud Filter in the Tropics

The performance of the cloud filter in the tropics was examined using night-time data only. AMSU/MHS T_B^{18} observed under cloudy skies are colder than those recorded in cloud-free conditions, and are much lower than the corresponding ARTS-simulated brightness temperatures. In Figure 2a, cloudy data points are located at the bottom-left section of the plot. The cloud filtered data are shown in Figure 2b. As the figure demonstrates, the cloud filter indeed removes most outliers and greatly improves the agreement between satellite and radiosonde. The cloud filter also performed equally well in comparisons made for all other radiosonde-satellite pairs (not shown).

4.2. Solar Radiation Dry Bias

Partitioning the radiosonde data into day and night profiles allows us to investigate the day-time dry bias that particularly the RS92 sondes are expected to have due to solar

radiation. We define night-time and day-time as follows: Night-time refers to the period between one hour after sunset and one hour before sunrise, and day-time to between one hour after sunrise and one hour before sunset. For night-time collocations, AMSU/MHS data may be within ± 1 hour of sunrise or sunset as long as the radiosonde-time is at night. This is reasonable as the satellite measurements are not influenced by solar radiation.

Averaged collocation time for each satellite-station pair is shown in Figure 3 (symbols denote the average collocation time and vertical bars its standard deviation). Figure 2b and c show night-time and day-time comparisons, respectively. For the TWP-C1/N17 pair, the collocations take place around 10 AM or 10 PM. The relative bias of the radiosonde data, in humidity space, compared to satellite measurement is 8.3% at night and 24.9% during the day. This corresponds to about 16.6% dry bias caused by solar heating.

Radiation dry bias and the difference between day and night biases for all satellite-station pairs are given in the last columns of Table 5. The radiation dry bias is $5-20\%$ which is consistent with the dry bias reported in *Vömel et al.* [2007]. The SGP-C1/N15, TWP-C3/N17, and TWP-C3/MA combinations show a smaller radiation dry bias, about $5-8\%$. This may be explained as the day/night differences are not substantial for these combinations, as can be inferred from Figure 3. This is in agreement with a smaller dry bias (maximum of 4%) estimated by *John and Buehler* [2005] for radiosonde data for 2001–2003 from European stations using N15 (7:30 AM/PM collocations) and a larger dry bias using N16 (1:30 AM/PM collocations) which was on average 9.6% for RS80 and 11.5% for RS90 sensors. The results are also consistent with the findings of *Miloshevich et al.* [2009] that RS92 day time biases are from $5-15\%$ in the $500-200$ hPa layer.

4.3. One-to-One Comparison

For the analysis presented in this section we use only cloud cleared night-time data. The number of collocations per year for each station/satellite pair is reported in Table 3. We use mainly the RS92 data (compare Table 2) for our analysis, but RS90 data for the N17/SGP-C1 combination is also quoted in Tables 4 and 5 for comparison. Combinations of 50 data points or more are used for the analysis. We describe the comparison with the help of statistical parameters including bias, standard deviation of the bias (σ_{bias}), slope, root mean square deviation (RMSD) and correlation coefficient. They are shown in Table 4 (radiance space) and in Table 5 (humidity space) for all available station/satellite combinations. Further details on calculating these quantities are given in Appendix A and in *Buehler et al.* [2004].

All station/satellite combinations show a negative bias in Table 4 and a positive bias in Table 5. In other words, the satellite UTH is moister than the radiosonde UTH. This is consistent with earlier studies, e.g., *Buehler et al.* [2008], *John and Buehler* [2005], and *Buehler and John* [2005]. The bias is between -0.6 and $-1.6\,\mathrm{K}$ in radiance space and between 1.1 and 2.4 %RH in humidity space ($5.1 - 15.4\%$ relative difference). For the SGP-C1/N17 combination, RS90 Bias (4.5 %) is less than RS92 bias (7.5 %) in humidity space. This is not consistent with *Miloshevich et al.* [2006a]. However, they reported that the accuracy of the RS92 data in the middle or upper troposhere, for temperatures between $-20\,^{\circ}\mathrm{C}$ and $-50\,^{\circ}\mathrm{C}$, is about 10%RH, Table 3 of *Miloshevich et al.* [2006a]. Therefore, the difference between RS90 and RS92 bias is still less than the accuracy of the radiosonde UTH. TWP-C3 shows a larger bias (-1.6 and $-1.5\,\mathrm{K}$) compared to other stations. This is due to the atmospheric conditions, as the average UTH at this station is

very low (25 %RH) compared to the average UTH at the other stations. Table 4 contains two additional bias parameters, D240 and D270, to make this last point clearer. These are the differences of the linear fit from the diagonal at 240 K and 270 K in the radiance space scatter plot. In contrast to the traditional bias (defined as the weighted mean of the difference) these bias parameters do not depend on the different mean conditions at the different stations. They show that TWP-C3 is indeed consistent with the other stations. Similar bias parameters D0% and D60% were added to the humidity space data in Table 5.

In humidity space, the slopes are close to unity and range between 0.94 to 1.05. In dry conditions, satellite UTH is moister than radiosonde UTH for all cases. This is consistent with the results from *Buehler et al.* [2004] and *John and Buehler* [2005]. During moist conditions, satellite UTH is sometimes more humid than radiosonde UTH, and sometimes drier. This can be seen in Table 5, where satellite-radiosonde combinations with a slope larger than 1 indicate moister satellite measurements than radiosondes. The correlation coefficients are very significant in all the cases and range from 0.97 to 0.99 in radiance space. Another very useful statistical parameter that reflects all other parameters is the weighted root mean square deviation (RMSD), defined in Appendix A. This parameter is presented in both radiance space (Table 4) and humidity space (Table 5). Radiance space RMSD ranges from 1.3 K for TWP-C2/N17 to 2.1 K for TWP-C3/N17. Humidity space RMSD ranges from 2.0 %RH for TWP-C3/N17 and TWP-C3/MA to 3.6 %RH for TWP-C1/N17 and TWP-C1/MA.

We also performed a statistical t-test to evaluate the difference between satellite and radiosonde UTH. We used a paired t-test because both satellite and radiosonde UTH are

observed under similar conditions. The results are shown in Table 4. The critical t-value at 0.05 confidence level is around 1.97, so in all cases t_{score} is larger than the critical t-value and the null hypothesis fails. Thus, although the bias is small, it is statistically significant.

One known source of bias is that our radiative transfer simulation neglects absorption by ozone (and also by other gases in the stratosphere, since the radiosonde profiles were cut at 100 hPa). According to Figure 3 of *John and Buehler* [2004], this will introduce a radiance dependent bias with approximately D240 = −0.15 K and D270 = −0.37 K. This means that up to approximately one fourth or a third of the observed bias can be explained by this effect.

A large part of the remaining bias is likely to be due to the radiosonde data, for example, the effect of contamination on the radiosonde data as shown by *Wang et al.* [2002], which causes a dry bias for the radiosonde data. In addition, *Soden et al.* [2004] and *Miloshevich et al.* [2006b] showed that radiosondes underestimate UTH for very dry conditions and introduced correction procedures to rectify deficiencies in the radiosonde humidity.

Another source of error is time-lag of the humidity sensor at cold temperatures [*Vömel et al.*, 2007; *Wang et al.*, 2002]. The relative humidity sensor response time increases exponentially with decreasing temperature and the consequence error can be as large as ±20 %RH at −40 °C and ±40 %RH at −70 °C if the ambient RH changes rapidly [*Miloshevich et al.*, 2001].

Of course the satellite data themselves also contribute possible sources of bias. Most notable here are a possible contamination by ice clouds that are not detected by the cloud filter and calibration issues of the satellite data.

4.4. Radiosonde Homogeneity and General Comparison Features

Overall, the ARM radiosonde data used in this study are considerably more homogeneous than the all-European radiosonde data that were used in *John and Buehler* [2005]. In that study, the bias at 245 K was found to vary approximately from −1.5 K to +1 K between the different stations for the same satellite. (The definition of the bias used there was similar to our D240, except for the small difference in reference temperature, which can be neglected here.)

For the ARM stations and night-time RS92 data, the D240 for the N17 satellite ranges only from −0.61 K to −0.26 K. We attribute this very good result mainly to the fact that the same sensor was used for all data. For the station SGP-C1 we also have RS90 data from early years (see Table 2). Indeed, for those data the D240 with the N17 satellite is +0.66 K, distinctly different from all other N17 comparisons.

The ARM data set is homogeneous enough to combine all data for the N17 satellite into a single scatter plot, as shown in Figure 4. Combined statistical parameters for all stations for N17 and other satellites are also included in Tables 4 and 5.

4.5. Monthly gridded UTH

We also compared the monthly averages of the radiosonde UTH to the matching cell of the monthly mean gridded AMSU/MHS UTH data. The monthly data set was originally developed by *Buehler et al.* [2008] and has been updated regularly. The grid size of this database is 2.5×2.5 degrees. We limited the comparison to the months with at least 25 radiosonde profiles. This threshold was estimated with respect to the accuracy of the monthly mean, i.e., $\sigma/\sqrt{n}$. The standard deviation, σ, was more or less equal to 5 %RH, see Table 6, and we assumed an accuracy of about 1 %RH, so $n = (5 \div 1)^2 = 25$. We

separated data into day and night to investigate the impact of radiation dry bias on monthly comparisons; we used the same definition as for the one-to-one comparison for day and night periods. Monthly means were calculated by averaging individual profiles. We collocated night-time/day-time monthly mean UTH to corresponding gridded data from descending/ascending orbits of N15, N16 and N18 and vice versa for N17 and MA. The statistics of this comparison, including bias (in %RH), relative bias (bias%) and slope (in %RH) are reported in Table 6. The night-time bias is less than 3.3 %RH or 10% in relative difference. In relative difference, the TWP-C1/N17 combination shows the lowest bias which is just -0.2%. For night-time data, the slope is nearly always less than one and ranges from 0.65 (TWP-C1/N15) to 1.02 (TWP-C2/N18).

Standard deviations of satellite gridded data and monthly averaged radiosonde data are reported in Table 6 and are quite similar. The standard deviation ranges from 3.9 (SGP-C1/N18) to 7.3 (TWP-C2/MA) for radiosonde data and from 3.5 (SGP-C1/N15) to 7.1 (TWP-C2/MA) for satellite data. Long-term averages of satellite and radiosonde UTH are also included. The long-term averages of SGP–C1, TWP–C1 and TWP–C2 for night-time radiosonde data are approximately $32.7 - 34.4$, $44.2 - 46.6$ and $33.8 - 36.8$ %RH, respectively.

The long-term averages, which are from combinations of recent satellites are less than those from older ones. For instance, at TWP–C2, the mean UTH has decreased from 36.0 for N15 to 33.8 for MetOp-A. We can not see this lapse in satellite UTH. To investigate this, annual variations of radiosonde UTH are shown in Figure 5 and a decrease in annual average of radiosonde UTH is evident in recent years, although ultimately the lapse is not particularly large.

We performed a t-test, see Table 6, to statistically compare the averages of monthly gridded data and monthly averaged radiosonde data. We argue that the satellite–radiosonde data are paired because both are influenced by the same weather conditions. The null hypothesis is that monthly averages of the gridded and radiosonde data are the same. For many station-satellite combinations, the differences are not statistically significant for the monthly gridded data, although they are significant in the one-to-one comparison. The reason for this apparent paradox is that the dominant error in the monthly comparison is the poor temporal sampling, particularly of the radiosonde data. The sampling problem leads to large random variations that mask the small systematic differences. The monthly comparison does not indicate a significant difference for the following satellite–station combinations: SGP-C1/N16, SGP-C1/MA, TWP-C1/N17, TWP-C1/MA, TWP-C2/N15, and TWP-C2/MA. We did not have enough data points for TWP–C3 station, thus this station is not included in Table 6.

Relative biases for day and night-time data are also reported in Table 6. The difference between night and day-time bias is between $7 - 23\%$. MetOp-A combinations show the largest differences because the radiosonde data of these combinations are from recent years which are recorded using RS92 sensors. For day-time data the relative bias ranges from 6% for SGP-C1/N15 to 27% for TWP-C2/MA combination. To date, radiosonde-satellite data comparisons performed by other researchers have not separated day/night biases, thus we calculated statistical parameters for combined day-night data. These parameters, including bias and relative bias, are also reported in Table 6. In this case, the bias ranges from 0.1 %RH for SGP-C1/N15 to 5.0 %RH for TWP-C2/N18. This corresponds to a

relative bias of 0.7% and 15.9% respectively. The slope is larger than 0.8 (SGP-C1/N15) and smaller than 1.1 (TWP-C1/MA, TWP-C2/N18 and TWP-C2/MA).

Buehler et al. [2008] initially validated this monthly gridded UTH at four stations located in different latitudes from sub-tropical, 15.93 °N, to high latitudes, 60.14 °N. They reported that for N16 the bias ranges from −4.33 to +4.90 %RH, the standard deviation is less than 3 %RH and the correlation coefficients is above 0.85. For the current comparison, the AMSU N16 bias is less than those reported by *Buehler et al.* [2008] and ranges between 1.5 and 3.1 %RH.

5. Summary and Conclusions

Although several studies have compared AMSU/MHS derived UTH with radiosonde data, none have done so for the tropics. We compared the brightness temperature and upper tropospheric humidity, UTH, retrieved from AMSU/MHS radiances, with the ARM radiosonde data of the tropical stations TWP-C1, -C2 and -C3 and the sub-tropical station SGP-C1.

We excluded radiosonde profiles measured during day-time because of the radiation dry bias. Several researchers have shown that Vaisala radiosondes, especially RS90 and RS92, have a large dry bias for daytime soundings (up to 50% in the upper troposphere) that is caused by solar heating of the RH sensor [*Vömel et al.*, 2007; *Miloshevich et al.*, 2006b; *Wang et al.*, 2002]. Our own study confirmed this strong radiation dry bias for day-time radiosonde data, particularly RS92.

Microwave radiances are largely insensitive to clouds. However, thick ice clouds are known to have some influence on measurements. We therefore employed a cloud filter

which is based on AMSU/MHS humidity channels. The performance of this filter was qualitatively evaluated and confirmed in the tropics.

The main comparison was done for cloud free night time data with a time difference of less than 2 hours between radiosonde and satellite. Additionally, a displacement filter discarded data when the product of wind speed and time difference was larger than 50 km.

We find good agreement between measured and simulated UTH with root mean square deviation (RMSD) less than 3.6 %RH and mean difference (bias) less than 2.4 %RH. The bias is small, but statistically significant. We attribute it to several sources. Part of the bias (up to about one third) can be explained by our omission of ozone absorption (and the entire stratosphere) from the radiative transfer calculations. Apart from that, the most important factor is likely to be the limited accuracy of the radiosondes, but uncertainties in the absolute calibration of the satellite data may also play a role.

It should be noted that this level of agreement would have been considered spectacularly good only a few years ago, when the typical level of agreement in such studies was several tens of percent, rather than a few percent [*Soden et al.*, 2004]. There are three main factors that contribute to the good agreement. The first factor is the improved quality of the radiosonde data, particularly in this study where all data were from the same sensor type. The second factor is the methodology to use a radiative transfer model to map the radiosonde data to radiance space, and then treat it in the same way as the satellite data. The third factor is careful collocation with appropriate filters to exclude cases where the comparison is not valid.

Besides the one-to-one comparison, we also compared monthly gridded satellite UTH against ARM radiosonde data. In that case the absolute value of the relative bias of

the night-time comparison ranged from 0.2 to 9.7%. Some station-satellite combinations showed a negative bias and others showed a positive bias.

While the results of the one-to-one comparison and the gridded monthly mean comparison are consistent, they are of quite different practical value. According to a t-test, the difference between satellite and radiosonde UTH is statistically significant for all one-to-one combinations, but only for some of the gridded monthly mean combinations. The reason for this is that the level of agreement between the two data sets is so good that the gridded monthly mean data comparison is dominated by sampling errors.

This finding has repercussions for future satellite validation studies. As data quality improves, collocation requirements become more and more stringent. This trend is likely to continue, so we foresee that a growing fraction of the total effort in future studies will be spent on carefully collocating the data, or in planing measurement campaigns to deliver coincident data.

Appendix A: Statistics

The bias is defined as the weighted mean of the differences between satellite T_b/UTH (T_{sat}/UTH_{sat}) and sonde T_b/UTH (T_{snd}/UTH_{snd}):

$$Bias = \frac{\sum w.\Delta B}{\sum w} \tag{A1}$$

where, $\Delta B = T_{sat} - T_{snd}$ or $\Delta B = UTH_{sat} - UTH_{snd}$ and $w = 1/\sigma^2$, σ is the standard deviation of the pixels located inside the target area, see Section 3.3. Similarly, relative bias ($Bias\%$) is defined as the weighted mean of the relative differences ($\Delta B\% = (T_{sat} -$

403 $T_{snd})/T_{snd}$ or $\Delta B\% = (UTH_{sat} - UTH_{snd})/UTH_{snd})$. $Bias\%$ is calculated using Equation
404 A1 but ΔB is replaced with $\Delta B\%$.

Standard deviation of the bias (σ_{bias}) is calculated as follows:

$$\sigma_{bias} = \sqrt{\frac{1}{\sum w}} \tag{A2}$$

Distance between the regression line and the diagonal line at the reference points, D240, D270, D0% and D60%, is calculated as follows:

$$D = a + (b - 1) \cdot x_{ref} \tag{A3}$$

405 where a and b are offset and slope of the fitted line and are calculated separately in radiance
406 and humidity space. x_{ref} is the reference point at which the distance is calculated and is
407 equal to 240, 270, 0 and 60 for D240, D270, D0% and D60%, respectively.

The root mean square deviation (RMSD) is defined as follows:

$$RMSD = \sqrt{\frac{\sum w.\Delta B^2}{\sum w}} \tag{A4}$$

408 **Acknowledgments.** Radiosonde data were obtained from the Atmospheric Radia-
409 tion Measurement (ARM) Program sponsored by the U.S. Department of Energy, Of-
410 fice of Science, Office of Biological and Environmental Research, Climate and Environ-
411 mental Sciences Division. Thanks to the ARTS radiative transfer community, many of
412 whom have indirectly contributed by implementing features to the ARTS model. Thanks
413 to Patrick Eriksson, Larry Miloshevich and David Parker for their comments. Special
414 thanks to Oliver Lemke for his assistance. Thanks to Lisa Neclos from the Comprehensive
415 Large Array-data Stewardship System (CLASS) of the US National Oceanic and Atmo-
416 spheric Administration (NOAA) for providing the AMSU data. Viju John was supported

417 by the U.K. Joint DECC and DEFRA Integrated Climate Programme - DECC/Defra
418 (GA01101). Isaac Moradi is financed by the Swedish Space Board, grant 48/09.

References

419 Bonsignori, R. (2007), The microwave humidity sounder (MHS): in-orbit performance
420 assessment, p. 67440A, SPIE Digital Library, doi:10.1117/12.737986.

421 Buehler, S. A., and V. O. John (2005), A simple method to relate microwave radi-
422 ances to upper tropospheric humidity, *J. Geophys. Res.*, *110*, D02110, doi:10.1029/
423 2004JD005111.

424 Buehler, S. A., M. Kuvatov, V. O. John, U. Leiterer, and H. Dier (2004), Comparison of
425 microwave satellite humidity data and radiosonde profiles: A case study, *J. Geophys.*
426 *Res.*, *109*, D13103, doi:10.1029/2004JD004605.

427 Buehler, S. A., P. Eriksson, T. Kuhn, A. von Engeln, and C. Verdes (2005), ARTS, the
428 atmospheric radiative transfer simulator, *J. Quant. Spectrosc. Radiat. Transfer*, *91*(1),
429 65–93, doi:10.1016/j.jqsrt.2004.05.051.

430 Buehler, S. A., M. Kuvatov, T. R. Sreerekha, V. O. John, B. Rydberg, P. Eriksson, and
431 J. Notholt (2007), A cloud filtering method for microwave upper tropospheric humidity
432 measurements, *Atmos. Chem. Phys.*, *7*(21), 5531–5542.

433 Buehler, S. A., M. Kuvatov, V. O. John, M. Milz, B. J. Soden, and D. L. J. aand J. Notholt
434 (2008), An upper tropospheric humidity data set from operational satellite microwave
435 data, *J. Geophys. Res.*, *113*, D14110, doi:10.1029/2007JD009314.

436 Cess, R. D., G. L. Potter, J. P. Blanchet, G. J. Boer, A. D. Del Genio, M. Déqué, V. Dym-
437 nikov, V. Galin, W. L. Gates, S. J. Ghan, J. T. Kiehl, A. A. Lacis, H. Le Treut, Z. X. Li,

X. Z. Liang, B. J. McAvaney, V. P. Meleshko, J. F. B. Mitchell, J. J. Morcrette, D. A. Randall, L. Rikus, E. Roeckner, J. F. Royer, U. Schlese, D. A. Sheinin, A. Slingo, A. P. Sokolov, K. E. Taylor, W. M. Washington, R. T. Wetherald, I. Yagai, and M. H. Zhang (1990), Intercomparison and interpretation of climate feedback processes in 19 atmospheric general circulation models, *J. Geophys. Res.*, *95*, doi:10.1029/JD095iD10p16601.

de F. Forster, P. M., and M. Collins (2004), Quantifying the water vapour feedback associated with post-Pinatubo global cooling, *Climate Dynamics*, *23*, 207–214.

Elliott, W. P., and D. J. Gaffen (1991), On the utility of radiosonde humidity archives for climate studies, *Bull. Amer. Met. Soc.*, *72*(10), 1507–1520.

Gettelman, A., and Q. Fu (2008), Observed and simulated upper-tropospheric water vapor feedback, *J. Climate*, *21*(13), 3282–3289, doi:10.1175/2007JCLI2142.1.

Gettelman, A., W. D. Collins, E. J. Fetzer, A. Eldering, F. W. Irion, P. B. Duffy, and G. Bala (2006), Climatology of upper-tropospheric relative humidity from the atmospheric infrared sounder and implications for climate, *J. Climate*, *19*(23), 6104–6121, doi:10.1175/JCLI3956.1.

Goodrum, G., K. B. Kidwell, and W. Winston (2007), NOAA KLM user's guide, *Tech. rep.*, National Environmental Satellite, Data, and Information Services (NESDIS).

John, V. O., and S. A. Buehler (2004), The impact of ozone lines on AMSU-B radiances, *Geophys. Res. Lett.*, *31*, L21108, doi:10.1029/2004GL021214.

John, V. O., and S. A. Buehler (2005), Comparison of microwave satellite humidity data and radiosonde profiles: A survey of European stations, *Atmos. Chem. Phys.*, *5*, 1843–1853, sRef-ID:1680-7324/acp/2005-5-1843.

John, V. O., and B. J. Soden (2007), Temperature and humidity biases in global climate models and their impact on climate feedbacks, *Geophys. Res. Lett.*, *34*, L18704, doi: 10.1029/2007GL030429.

John, V. O., S. A. Buehler, and N. Courcoux (2006), A cautionary note on the use of gaussian statistics in satellite based UTH climatologies, *IEEE Geosci. R. S. Le.*, *3*(1), 130–134, doi:10.1109/LGRS.2005.859350.

Miloshevich, L. M., H. Vömel, A. Paukkunen, A. J. Heymsfield, and S. J. Oltmans (2001), Characterization and correction of relative humidity measurements from Vaisala RS80-A radiosondes at cold temperatures, *J. Atmos. Oceanic Technol.*, *18*(2), 135–156.

Miloshevich, L. M., H. Vömel, D. N. Whiteman, B. M. Lesht, F. J. Schmidlin, and F. Russo (2006a), Absolute accuracy of water vapor measurements from six operational radiosonde types launched during awex-g and implications for airs validation, *J. Geophys. Res.*, *111*(D9), doi:10.1029/2005JD006083.

Miloshevich, L. M., H. Vömel, D. N. Whiteman, B. M. Lesht, F. J. Schmidlin, and F. Russo (2006b), Absolute accuracy of water vapor measurements from six operational radiosonde types launched during AWEX-G and implications for AIRS validation, *J. Geophys. Res.*, *111*(D09S10), 953–963, doi:10.1029/2005JD006083.

Miloshevich, L. M., H. Vomel, D. N. Whiteman, and T. Leblanc (2009), Accuracy assessment and correction of vaisala rs92 radiosonde water vapor measurements, *J. Geophys. Res.*, *114*, D11305, doi:10.1029/2008JD011565.

Minschwaner, K., and A. E. Dessler (2004), Water vapor feedback in the tropical upper troposphere: Model results and observations, *J. Climate*, *17*(6), 1272–1282, doi:10.1175/1520-0442(2004)017$⟨$1272:WVFITT$⟩$2.0.CO;2.

Saunders, R. W., T. J. Hewison, S. J. Stringer, and N. C. Atkinson (1995), The radiometric characterization of AMSU-B, *IEEE T. Microw. Theory*, *43*(4), 760–771.

Soden, B. J., and F. P. Bretherton (1993), Upper tropospheric relative humidity from the GOES 6.7 μm channel: Method and climatology for july 1987, *J. Geophys. Res.*, *98*(D9), 16,669–16,688.

Soden, B. J., and J. R. Lanzante (1996), An assessment of satellite and radiosonde climatologies of upper-tropospheric water vapor, *J. Climate*, *9*, 1235–1250.

Soden, B. J., D. D. Turner, B. M. Lesht, and L. M. Miloshevich (2004), An analysis of satellite, radiosonde, and lidar observations of upper tropospheric water vapor from the atmospheric radiation measurement program, *J. Geophys. Res.*, *109*, D04105, doi: 10.1029/2003JD003828.

Soden, B. J., D. J. Jackson, V. Ramaswamy, M. D. Schwarzkopf, and X. Huang (2005), The radiative signature of upper tropospheric moistening, *Science*, *310*(5749), 841–844, doi:10.1126/science.1115602.

Stokes, G., and S. Schwarts (1994), The Atmospheric Radiation Measurement (ARM) program - programmatic background and design of the cloud and radiation test-bed, *Bull. Amer. Met. Soc.*, *75*(7), 1201–1221.

Turner, D. D., B. M. Lesht, S. A. Clough, J. C. Liljegren, H. E. Revercomb, and D. C. Tobin (2003), Dry bias and variability in vaisala RS80-H radiosondes: The ARM experience, *J. Atmos. Oceanic Technol.*, *20*, 117–132.

Vömel, H., H. Selkirk, L. Miloshevich, J. Valverde-Canossa, J. Valdes, E. Kyroe, R. Kivi, W. Stolz, G. Peng, and J. A. Diaz (2007), Radiation dry bias of the Vaisala RS92 humidity sensor, *J. Atmos. Oceanic Technol.*, *24*(6), 953–963, doi:10.1175/JTECH2019.

1.

Wang, J. H., H. L. Cole, D. J. Carlson, E. R. Miller, K. Beierle, A. Paukkunen, and T. K. Laine (2002), Corrections of humidity measurement errors from the Vaisala RS80 radiosonde - Application to TOGA COARE data, *J. Atmos. Oceanic Technol.*, *19*(7), 981–1002, doi:10.1175/1520-0426(2002)019⟨0981:COHMEF⟩2.0.CO;2.

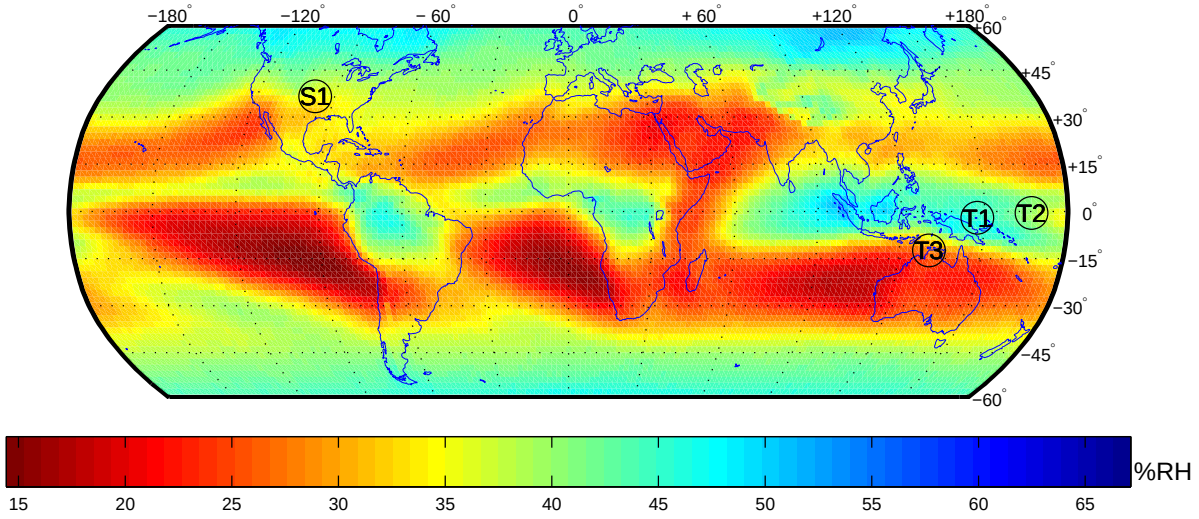

Figure 1. Location of the stations superimposed on the mean UTH map retrieved from N17 AMSU data for the period 2002-2009. T1, T2, T3 and S1 stand for TWP-C1, TWP-C2, TWP-C3 and SGP-C1 stations, respectively.

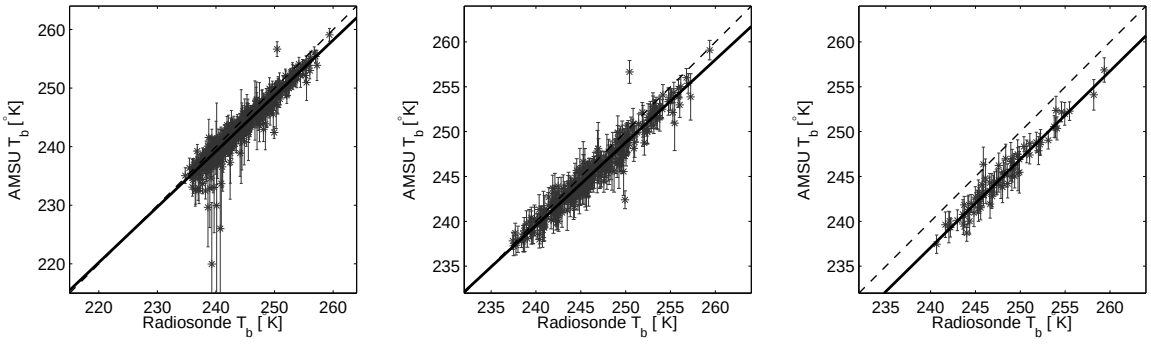

(a) Night time all skies (b) Night time clear skies (c) Day time clear skies

Figure 2. The scatter-plots of N17 AMSU T_b versus TWP-C1 T_b for the whole data. Vertical lines show the standard deviation of each data point given by the standard deviation of pixels inside the target area. The dashed and solid lines are diagonal and regression lines, respectively.

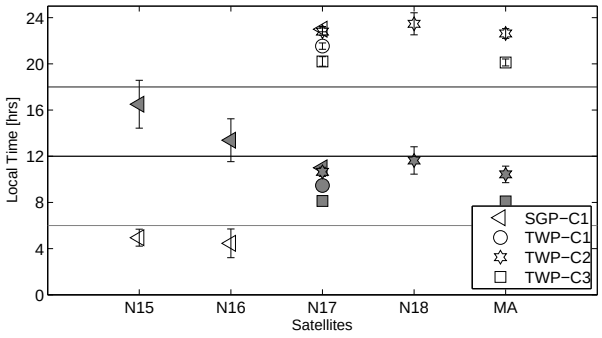

Figure 3. Average collocation time for different satellite-station pairs. Different stations are coded using different markers. Filled and unfilled markers stand for day-time and night-time, respectively.

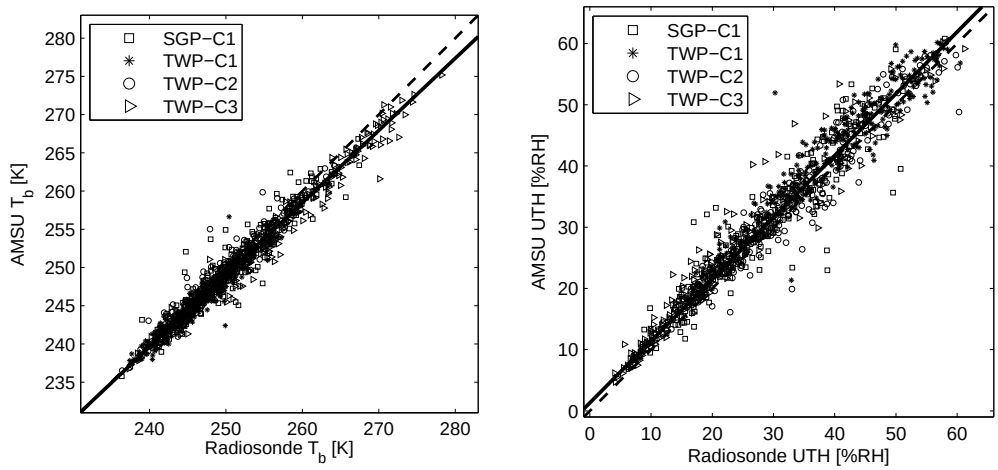

(a) (b)

Figure 4. Scatter plots of N17 AMSU data versus radiosonde RS92 data from all stations in radiance space (a) and humidity space (b). Different symbols mark different stations. The dashed line shows the diagonal, the solid line a linear fit.

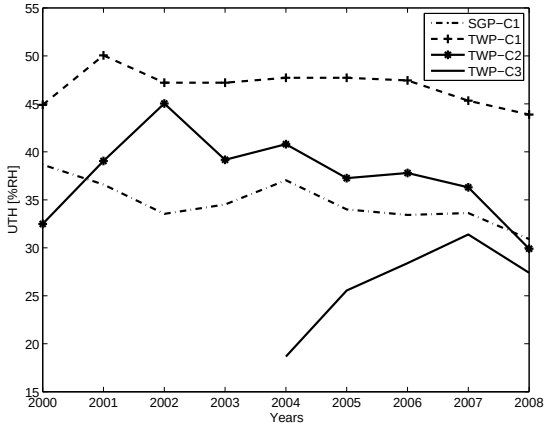

Figure 5. Annual variation of sonde UTH for different stations.

Table 1. Geographical attributes of the studied stations. The last two columns show mean and standard deviation of UTH for the night-time profiles of the period 2004-2008.

Station	Abbr.	latitude [deg.]	longitude [deg.]	Altitude [meters]	Operating since YYMM	$\overline{UTH}$ [%RH]	σ [%RH]
Southern Great Planes, Central Facility, Lamont, OK	SGP-C1	36.61	-97.49	315	0010	34.28	14.58
Tropical Western Pacific, Central Facility, Manus I., PNG	TWP-C1	-2.06	147.43	4	9708	44.17	12.39
Tropical Western Pacific, Central Facility, Nauru Island	TWP-C2	-0.52	166.92	7	9903	37.30	13.74
Tropical Western Pacific, Central Facility, Darwin, North Australia	TWP-C3	-12.42	130.88	30	0204	25.72	17.48

Table 2. Radiosonde sensors that have been used to measure humidity at different stations

station	RS80	RS90	RS92
SGP C1	0010–0104	0105–0502	0502–0812
TWP C1	9708–0205	0206–0503	0504–0812
TWP C2	9903–0205	0206–0503	0504–0812
TWP C3	0204–0601		0601–0812

Table 3. Number of available data points per year for night data. The matches with more than 50 data points are used for the conclusions. The combinations with less than 50 data-points, in total, are not shown

station	sat.	2001	2002	2003	2004	2005	2006	2007	2008	sum
SGP C1	N15	1	1	1	9	17	26	59	40	154
SGP C1	N16	1	31			3	28	81	43	187
SGP C1	N17		36	60	90	101	60	48	11	406
TWP C1	N17		3	6	7	8	42	133	112	311
TWP C1	MA						14	150	113	277
TWP C2	N17			5	4	4	27	131	98	269
TWP C2	MA						6	77	48	131
TWP C2	N18					3	5	21	30	59
TWP C3	N17				8	6	59	79	73	225
TWP C3	MA						18	124	99	241

Table 4. Statistical parameters for AMSU/MHS T_b minus Radiosonde T_b. The slope, bias, standard deviation of the bias (σ_{bias}) and root mean square deviation (RMSD) are in Kelvin. The columns D240 and D270 show the distance between the regression line and the diagonal line, in Kelvin, at 240 and 270 K sonde brightness temperature. N is the number of data points used to calculate the statistics and r is the correlation coefficient. The parameter t_{score} is the t-score of a paired t-test. For SGP-C1/N17 the first line shows data from RS92 and the second line data from RS90. (All other data are RS92.) The last rows show statistics calculated using RS92 data from all the stations but for different satellites.

Station	Sat.	Slope	r	Bias	%Bias	D240	D270	σ_{bias}	RMSD	t_{score}	N
SGP-C1	N15	0.92	0.98	-0.59	-0.23	0.22	-2.13	0.16	1.37	5.63	141
SGP-C1	N16	0.94	0.98	-0.90	-0.35	-0.27	-1.98	0.16	1.62	8.21	155
SGP-C1	N17	0.97	0.97	-0.87	-0.35	-0.55	-1.42	0.10	1.79	8.21	216
SGP-C1 RS90	N17	0.90	0.97	-0.26	-0.10	0.66	-2.29	0.10	1.71	2.08	190
TWP-C1	N17	0.92	0.97	-0.93	-0.37	-0.46	-2.73	0.07	1.44	14.51	295
TWP-C1	MA	0.94	0.98	-0.84	-0.34	-0.54	-2.22	0.06	1.33	13.58	277
TWP-C2	N17	0.96	0.98	-0.61	-0.24	-0.26	-1.35	0.08	1.28	8.74	260
TWP-C2	N18	1.00	0.98	-1.04	-0.42	-1.03	-1.04	0.13	1.47	7.59	59
TWP-C2	MA	0.99	0.98	-0.81	-0.33	-0.71	-1.05	0.08	1.38	8.39	131
TWP-C3	N17	0.94	0.99	-1.64	-0.63	-0.61	-2.34	0.09	2.12	17.68	211
TWP-C3	MA	0.96	0.99	-1.54	-0.59	-0.81	-2.12	0.06	1.93	20.30	241
ALL-DATA	N15	0.92	0.98	-0.59	-0.23	0.22	-2.13	0.16	1.37	5.63	141
ALL-DATA	N16	0.94	0.98	-0.90	-0.35	-0.27	-1.98	0.16	1.62	8.21	155
ALL-DATA	N17	0.94	0.99	-0.99	-0.39	-0.39	-2.07	0.04	1.63	23.66	982
ALL-DATA	N18	1.00	0.98	-1.04	-0.42	-1.03	-1.04	0.13	1.47	7.59	59
ALL-DATA	MA	0.95	0.99	-1.08	-0.43	-0.59	-2.04	0.04	1.57	23.89	649

Table 5. Statistical parameters for AMSU/MHS UTH minus Radiosonde UTH. Slope, bias, standard deviation of the bias (σ_{bias}) and root mean square deviation (RMSD) are in %RH. Subscript d stands for day-time data, all other data are night-time. N shows the number of data points and $\Delta B = \%Bias - \%Bias_d$. The columns D0% and D60% show the distance between the regression line and the diagonal line, in %RH, at 0 %RH and 60 %RH sonde UTH values. N is the number of data points used to calculate the statistics and r is the correlation coefficient. The parameter t_{score} is the t-score of a paired t-test. For SGP-C1/N17 the first line shows data from RS92 and the second line data from RS90. (All other data are RS92.) The last rows show statistics calculated using RS92 data from all the stations but for different satellites.

Station	Sat.	Slope	r	Bias	%Bias	D0%	D60%	σ_{bias}	RMSD	N	$Bias_d$	$\%Bias_d$	N_d	ΔB
SGP-C1	N15	0.94	0.98	1.30	8.38	2.58	-1.09	0.28	2.38	141	2.24	16.82	121	8.44
SGP-C1	N16	0.98	0.98	1.60	9.40	1.99	0.86	0.26	2.70	155				
SGP-C1	N17	0.99	0.96	1.28	7.48	1.40	1.03	0.15	2.93	216	4.34	25.16	708	17.68
SGP-C1 RS90	N17	0.91	0.96	0.60	4.45	2.68	-2.78	0.17	3.08	190	3.44	18.51	498	14.06
TWP-C1	N17	0.97	0.97	2.35	8.32	3.34	1.55	0.17	3.57	295	7.18	24.92	78	16.60
TWP-C1	MA	0.99	0.98	2.22	7.45	2.68	1.88	0.13	3.56	277				
TWP-C2	N17	0.99	0.97	1.10	5.10	1.31	0.80	0.14	2.55	260	5.14	24.51	87	19.41
TWP-C2	N18	1.05	0.98	1.79	7.58	0.53	3.63	0.22	2.85	59	4.43	22.07	60	14.49
TWP-C2	MA	1.02	0.98	1.40	5.78	0.79	2.25	0.14	2.71	131	4.56	21.39	104	15.61
TWP-C3	N17	1.04	0.98	1.50	15.35	1.06	3.48	0.09	2.00	211	2.42	22.13	324	6.78
TWP-C3	MA	1.05	0.99	1.53	14.35	0.97	3.73	0.07	2.04	241	2.35	19.76	183	5.41
ALL-DATA	N15	0.94	0.98	1.30	8.38	2.58	-1.09	0.28	2.38	141	2.24	16.82	121	8.44
ALL-DATA	N16	0.98	0.98	1.60	9.40	1.99	0.86	0.26	2.70	155				
ALL-DATA	N17	1.01	0.99	1.50	10.94	1.32	1.91	0.06	2.55	982	3.51	23.63	119	12.69
ALL-DATA	N18	1.05	0.98	1.79	7.58	0.53	3.63	0.22	2.85	59	4.53	25.21	168	17.63
ALL-DATA	MA	1.02	0.99	1.63	11.68	1.20	2.62	0.06	2.50	649	3.31	21.56	426	9.88

Table 6. Statistical parameters for monthly gridded AMSU/MHS UTH vs. monthly Radiosonde UTH. The slope and bias are in $\%RH$. The columns are as follows: Sta is station, Sat is satellites, σ is standard deviation, $\overline{sonde}$ is long-term mean of sonde UTH, $\overline{sat}$ is long-term mean of satellite UTH, t_s is t score, N is number of collocated months, NP is total number of profiles, $\Delta B\%$ is the difference between day and night time biases and subscribes "d" and "a" refer to day and day and night together, respectively. First 12 columns represent parameters from night time data.

Station	Sat	Bias	Bias%	Slope	σ_{sonde}	σ_{sat}	$\overline{sonde}$	$\overline{sat}$	t_s	N	NP	Bias_d	$\text{Bias}_d\%$	Slope_d	N_d	$\Delta B\%$	Bias_a	$\text{Bias}_a\%$	Slope_a	N_a	NP_a
SGP C1	N15	-0.74	-1.66	0.68	4.48	3.51	34.39	33.65	2.89	80	3671	1.57	5.56	0.92	87	7.21	0.12	0.74	0.80	96	10060
SGP C1	N16	0.21	1.04	0.74	4.48	3.80	34.39	34.61	-0.87	80	3671	3.49	12.09	0.93	87	11.05	1.50	5.04	0.81	96	10060
SGP C1	N17	-0.54	-1.33	0.82	4.17	3.82	34.08	33.53	2.32	65	3671	4.61	16.36	0.84	72	17.69	1.76	5.95	0.81	77	10060
SGP C1	N18	1.52	4.83	0.90	3.92	4.04	32.88	34.40	-4.25	31	3671	5.20	18.77	1.14	39	13.93	3.20	10.71	0.98	42	10060
SGP C1	MA	0.46	1.68	0.84	4.17	4.05	32.67	33.13	-0.84	15	3671	4.96	18.30	0.71	21	16.62	2.28	7.80	0.86	24	10060
TWP C1	N15	-3.14	-6.44	0.65	4.82	3.78	46.57	43.43	8.23	49	2399	4.68	12.03	0.97	63	18.47	0.82	2.14	0.81	102	5386
TWP C1	N16	-1.43	-2.81	0.73	4.86	4.21	46.53	45.10	3.79	48	2399	4.80	12.46	0.82	61	15.27	1.94	4.69	0.80	93	5386
TWP C1	N17	-0.19	-0.24	0.84	4.56	4.19	45.96	45.78	0.64	42	2399	6.27	16.36	0.86	52	16.59	3.29	7.85	0.92	77	5386
TWP C1	N18	1.49	3.50	0.81	4.55	4.30	45.52	47.01	-3.57	32	2399	6.86	18.25	1.16	33	14.75	4.25	10.22	1.00	42	5386
TWP C1	MA	1.38	3.36	0.86	5.12	5.71	44.24	45.62	-1.56	18	2399	7.36	19.79	1.14	19	16.43	4.58	11.19	1.05	24	5386
TWP C2	N15	-0.02	0.67	0.78	6.60	5.57	36.03	36.01	0.06	51	2647	3.98	13.00	1.01	77	12.33	1.87	5.78	0.95	112	5692
TWP C2	N16	1.39	4.45	0.80	6.43	5.55	36.83	38.22	-3.74	44	2647	4.71	15.74	0.89	72	11.29	3.13	9.43	0.91	95	5692
TWP C2	N17	1.36	4.20	0.87	5.80	5.52	35.85	37.21	-3.39	34	2647	6.51	21.79	0.98	59	17.60	4.23	12.61	0.99	77	5692
TWP C2	N18	3.26	9.69	1.02	5.89	6.32	34.29	37.55	-7.74	22	2647	6.43	23.34	1.11	32	13.65	5.01	15.92	1.06	42	5692
TWP C2	MA	1.33	4.41	0.90	7.28	7.09	33.77	35.10	-1.49	10	2647	7.18	27.03	1.21	17	22.62	4.55	14.71	1.07	24	5692